Building a model for antenna aperture illumination pattern

Srikrishna Sekhar, Preshanth Jagannathan, Brian Kirk, Sanjay Bhatnagar and Russ Taylor

Feb. 2019

Executive Summary

The sensitivity of modern radio telescopes is high enough that imaging is often limited by the effects of variations in the antenna primary beams as a function of frequency, polarization, time or antenna. The `WB Full-polarization AW-Projection (WB-FP-AWP)` algorithm offers a method to correct for the effects of antenna primary beams, which requires an accurate model of the antenna aperture illumination patterns (AIP), as a function of time, frequency, and polarization. The AIP is usually referred to in the literature as the `A-term`. This report details the development of an algorithm to model the antenna aperture illumination pattern.

To model complex-valued aperture illumination patterns in full polarization an algorithm using Zernike Polynomials was tested against holographic measurements of the EVLA, ALMA and MeerKAT telescopes and demonstrated to achieve the required accuracy. Since this is a polynomial model, it is applicable to any type of antenna (as demonstrated by application to EVLA, ALMA and MeerKAT – which have very different type of antennas). The algorithm implementation was done in Python. More work is necessary to incorporate this work for use as part of the `WB-FP-AW-Projection` algorithm for imaging, which will enable its use for wide-field, wide-band, polarimetric imaging with MeerKAT.

Context for the work: The `AW-Projection` (AWP) algorithm is designed to project-out the effects of the antenna primary beams (PB), *i.e.,* the A term, and the W-term in the interferometric measurement equation as part of the transformation of the data to the image domain. This is achieved by incorporating the A- and the W-term while gridding the data on a regular grid before applying the FFT algorithm to transform it to the image domain. The resulting image is corrected for the effects of the A- and W-terms and can be supplied as the input to image-plane deconvolution algorithms, like the MS/MT-MFS algorithm to build a wide-band multi-scale model of the sky emission. These deconvolution algorithms are purely image-plane algorithms designed (and optimized) to model *only* the sky emission, and therefore have implicit assumptions of the input data being free of instrumental effects (like the effects of the A- and the W-terms). Combination of using the AWP algorithm to make the (dirty/residual) images and the MS/MT-MFS algorithm for constructing a model of the sky therefore provides a robust solution for wide-band wide-field full-polarization imaging.

The effects of A-term are rotationally asymmetric, which in-turn introduces significant gain variations as a function of time, frequency and polarization. The errors due to these variations are much larger than the typical sensitivity afforded by the collecting area and wide-band receivers of modern radio telescopes. The effects can be corrected using the AWP algorithm. However the AWP algorithm requires computation of the A- and W-terms during imaging. While the W-term is a geometric term and can be precisely computed, the A-term requires a mechanism that accurately captures the details of the antenna AIP in full polarization. Although the AIPs can be measured using the technique of holographic measurements, the signal-to-noise ratio (SNR) of these measurements is significantly lower than typical target observations. Developing an accurate model for the A-term based on holographic measurements is therefore necessary and also the primary focus of this work. The algorithm presented in this report will enable application of the AW-Projection implementation in CASA to any telescope (e.g. MeerKAT).

The technique: The antenna primary beams in Stokes-I are significantly rotationally asymmetric for blocked-aperture antennas (like those of the EVLA and ALMA). They are fundamentally asymmetric in Stokes-Q, -U and -V for all types of antennas due to projection effects. Briefly, due to the orthogonal orientation of the feed between the two polarizations, any signal that is received maximally in one polarization will be a minimum in the other. Therefore any cross-hand products are inherently asymmetric. These patterns also vary across the array due to antenna-to-antenna surface variations, independent antenna pointing errors or due to inherently heterogeneous arrays (like ALMA). Complex Zernike polynomials

were fit to the aperture planes of the three telescopes (generated from the PB holography measurements) by minimizing the χ^2 distance between the modeled and measured aperture illuminations. The resulting models, when transformed to the image-plane showed noise-like residuals out to PB side-lobes where the apparent brightness of the illuminating celestial source remained significant. The resulting model captures the asymmetries across the band in all Stokes PBs. When implemented as the A-term in the `AWP` algorithm, we expect it to correct for the effects of the time, frequency and polarization variations of the antenna PBs.

Results: The Zernike model when transformed to the image plane captures all the significant features in the Stokes-I PBs, including rotational asymmetries due to blocked aperture up to the 2^{nd} (for ALMA) and the 3^{rd} (for EVLA and MeerKAT) PB sidelobe. The expected Clover-leaf pattern in Stokes-Q and -U beams and the effect of polarization squint in Stoke-V (for EVLA and ALMA) was also clearly captured. Independent conformation of these results were done by comparing these results with the ray-tracing software already in use in CASA for the EVLA and ALMA antennas. This ray-traced model has been verified against real observations and shown to produce Stokes-I and -V images free of PB effects (Jagannathan 2018). The technique of Zernike modeling was applied to EVLA which measures in circular polarization basis, and also to ALMA and MeerKAT both of with measure in linear polarization basis. As can be trivially expected, the technique is independent of the polarization basis of the data.

The fitting was also done as a function of frequency across the band and the model captures the frequency variations accurately. These frequency variations are introduced due to standing waves in the antenna optics and due to feed illumination effects. Both these are hard to model via ray-tracing in a computationally efficient manner.

Future plan: In the immediate future, we plan to write up the work done already as a paper for publication in refereed journal. The AWP implementation in the production version of CASA is capable of reading the requisite information about telescope-specific A-term via a disk cache. For NRAO telescopes (EVLA and ALMA) the software to build this cache already exists in CASA. The Zernike polynomial software developed here will be used to build such a disk-cache for MeerKAT, which will be incorporated into the IDIA processing pipeline and will be made generally available to users of the IDIA cloud computing systems. The goal is to achieve this in the next few months. Since this is intricate work, Srikrishna will visit NRAO again later in the year. This will finish the work required for application of AWP algorithm for MeerKAT imaging in Stokes-I. Wide-band full-polarization imaging requires more work – both, in the AWP framework as well as on the image deconvolution part of the processing. Plan is for Srikrishna to visit NRAO for a longer visit starting in Q3 of 2019.

Chapter 1

Introduction

The measurement equation in it's most general form is given by (Bhatnagar et al. 2008)

$$V_{ij}^{obs} = \mathrm{M}_{\mathrm{ij}}^{\mathrm{DI}} \int \mathrm{M}_{\mathrm{ij}}^{\mathrm{DD}}(\tilde{\mathrm{s}})\mathrm{I}(\tilde{\mathrm{s}})\mathrm{e}^{2\pi i \tilde{\mathrm{s}}.\tilde{\mathrm{b}}_{\mathrm{ij}}} d\tilde{\mathrm{s}} \tag{1.1}$$

where V_{ij}^{obs} represent the observed visbilities of the source in the sky I, along a direction $\vec{s}$ as seen by the antenna baseline vector $\vec{b_{ij}}$. The Mueller matrices, $\mathrm{M}_{\mathrm{ij}}^{\mathrm{DI}}$ represent the direction independent gains and $\mathrm{M}_{\mathrm{ij}}^{\mathrm{DD}}$ the direction dependent gains, V_{ij}^{obs} the observed visbilities of the source. Direction dependent effects such as the antenna primary beam and the ionosphere are represented by $\mathrm{M}_{\mathrm{ij}}^{\mathrm{DD}}$. In the case of the antenna primary beam the Mueller matrix is constructed from the outer product of the Jones matrices measuring the primary beam voltage patterns $\mathrm{M}_{\mathrm{ij}} = \mathrm{J}_{\mathrm{i}} \otimes \mathrm{J}_{\mathrm{j}}^{*}$, where the Jones matrix is:

$$\mathrm{J}_i^{sky}(\mathbf{s}) = \begin{bmatrix} \mathrm{J}_i^{p} & -\mathrm{J}_i^{p \rightarrow q} \\ \mathrm{J}_i^{q \rightarrow p} & \mathrm{J}_{\mathrm{i}}^{\mathrm{q}} \end{bmatrix} \tag{1.2}$$

where p and q are the polarizations in the feed basis (either linear or circular), and $p \rightarrow q$ and $q \rightarrow p$ represent p leaking into q and vice-versa. Holography measurements are used to map the antenna Jones.

As both the A-Term ($\mathrm{M}_{\mathrm{ij}}^{\mathrm{DD}}$) and W term lie within the integral of the measurement equation, it is only possible to correct for them as a part of imaging. Post imaging corrections are fundamentally rued out. In order to correct for the A-Term we require accurate model of the antenna aperture illumation patterns. Antenna aperture illumination patterns are influenced by the antenna geometry, blockages, deformations of the dish surface among others. These effects cause the antenna primary beam to be rotationally asymmetric. Modelling the antenna aperture illumination pattern effectively across large bandwidths for all polarization is computationally expensive and algorithmically complex as demonstrated by Jagannathan et al. (2017) in the A-Solver approach. The current implementation of the A-solver perturbs the parameters of a ray traced VLA beam model to obtain the best fit to the measured holography. This method has been shown to work well for the VLA for two polarizations. The method fits for geometric parameters of antenna that are passed to ray-tracer, *i.e.,* the effective aperture blockage, the aperture illumination taper function and the pointing offset, and uses the Nelder-Mead simplex optimizer to minimize these parameters. This requires the ray-tracing code to be re-run at every iteration of the algorithm in order to minimize the model beam that is produced.

Here we describe a method that uses Zernike polynomials to model the antenna aperture illumination patterns. This method is more computationally efficient and eliminates the need for a ray traced model while providing a better fit to the holography data across all polarizations while remaining telescope and feed basis agnostic . In the following chapters of the report we will describe the holography data for MeerKAT, VLA, and ALMA, and demonstrate the efficacy of our Zernike polynomial method in modelling the aperture illumination pattern.

Chapter 2

Holography

Holographic measurements of an interferometric array are used to map the far-field voltage patterns of the antenna in the array. Eq 1.1 can be written in matrix form as :

$$V_{ij} = g_{ij} F(\mathrm{J_i} \otimes \mathrm{J_j}) S\, I^{sky} \tag{2.1}$$

where $\mathrm{V_{ij}}$ is the recorded visibility relates to the sky brightness distribution of the source I^{sky} through a Fourier transform, F as given by the van Cittert-Zernike theorem. g_{ij} are the nominal direction independent gains which are corrected for during calibration and S is a linear transform matrix that converts the sky brightness distribution in the Stokes basis to the antenna feed basis. The incoming sky brightness is altered by the antenna directional response given by the Jones matrices $\mathrm{J_i}$ and $\mathrm{J_j}$ for antennas i, j in a baseline $i - j$. The method we use to map the far-field voltage pattern is to observe a grid of offset locations around a strong unresolved(point source) calibrator with half the antennas pointed on source while the other half scan the grid locations. We do make the implicit assumption that all the antennas tracking the calibrator source are alike in their voltage patterns and are pointing at the same location on the sky. This simplifies the measurement equation which can then be written as,

$$V_{st} = g_{st} F(\mathrm{J_{scan}} \otimes \mathrm{J_{track}}) S\, I^{Sky} \tag{2.2}$$

where, $\mathrm{J_{scan}}$ represents the far field voltage pattern of the scanning antenna which we will determine and $\mathrm{J_{track}}$ is the tracking or reference antenna. The subscripts $_s$ and $_t$ also denote scanning and tracking antennas respectively. $\mathrm{J_{track}}$ in the ideal case of the antenna pointed at the calibrator can be written as

$$J_{track} = \begin{pmatrix} g^x & -D^{x\to y} \\ D^{y\to x} & g^y \end{pmatrix} \tag{2.3}$$

where g_x and g_y are the gains of the antenna in the linear basis and $Dx \to y, Dy \to x$ represents the coupling of the orthogonal feed basis. For an ideal tracking antenna $Dx \to y, Dy \to x = 0$ and $g_x, g_y = 1$ after calibration, which simplifies the Jones matrix in Eq:2.3 to $J_{track} = \mathbb{1}$. Under this simplifying assumption we can expand the terms and compute the outer product in Eq:2.2 to be

$$\frac{1}{g_{st}} \begin{pmatrix} V^{xx} \\ V^{xy} \\ V^{yx} \\ V^{yy} \end{pmatrix}_{st}^{Obs} = F \begin{pmatrix} J_x & -J_{x\to y} & 0 & 0 \\ J_{y\to x} & J_y & 0 & 0 \\ 0 & 0 & J_x & -J_{x\to y} \\ 0 & 0 & J_{y\to x} & J_y \end{pmatrix} S \begin{pmatrix} I \\ Q \\ U \\ V \end{pmatrix}^{sky} \tag{2.4}$$

Expanding $S \cdot I^{sky}$ and the Fourier transform in Eq:2.4, post calibration (applying the gains g_{ij}) we can arrive at a system of four linear equations in feed basis,

$$V^{xx} = J_x \cdot XX^{sky} - J_{x\to y} \cdot XY^{sky} \tag{2.5}$$
$$V^{xy} = J_{y\to x} \cdot XX^{sky} - J_y \cdot XY^{sky} \tag{2.6}$$
$$V^{yx} = J_x \cdot YX^{sky} - J_{x\to y} \cdot YY^{sky} \tag{2.7}$$
$$V^{yy} = J_{y\to x} \cdot YX^{sky} - J_y \cdot YY^{sky} \tag{2.8}$$

where $[XX^{sky}, XY^{sky}, YX^{sky}, YY^{sky}]^T$ is the sky brightness vector in feed basis and is a known quantity if the exact flux density of the calibrator is known to high precision in all the four Stokes bases. The observed visibilities across the scanning grid forms the left-hand-side of each of equations leaving four unknowns, i.e, the Jones matrix values that can be solved for. This was the primary procedure used to derive the Jones matrix for the antenna in the feed basis.

Some aspects of the system of equations requires a closer examination. If the source observed for holography is unpolarized i.e. $Q, U, V = 0$ the system of linear equations then would simply give us the four terms of the Jones matrix requiring no further computation. This additional simplification has been exploited in Holographic measurements at cm wavelengths at the VLA, ATCA, GMRT and WSRT. From the system of linear equations in its most general form for the tracking antennas that includes non-ideal feeds, the leakage is also a parameter that needs to be determined and increases the number of unknowns from 4 to 6 for our system of four linear equations. An effective means of measuring the leakage terms requires larger parallactic angle coverage to accurately estimate the $Dx \to y, Dy \to x$ at every off-axis location. At high frequencies where truly unpolarized bright sky sources are hard to find such as for ALMA

2.1 Observations and Data Processing

2.1.1 VLA

Holography data were taken for the VLA, ALMA at different times following similar methodologies. In this and the following section we will highlight the observing methodology and the data processing for the datasets. Both telescopes scanned a square grid around a bright sky calibrator source with one half of the antennas tracking the source and the other scanning the grid around the calibrator source. In the case of the VLA we were able to repeat the experiment with the scanning and tracking antennas groups reversed.

The VLA data were taken in September of 2015 at S-band($2-4$ GHz) of the VLA in a 57×57 grid spanning $73' \times 73'$ around the calibrator source 3C147 in a ten hour observing run. Nine antennas(3,5,7,18,20,26,27) were utilized reference antennas and were pointed the source at all times. Four other antennas (4,9,10,24) are not included in any of the observations and are consequently flagged in our visbility data. The visibility data were ingested into casa where extensive RFI flagging was performed. Four of the 16 spectral windows contained strong persistent RFI and so are not included in the beam image cubes that were produced. At the end of each row of the holography grid the central calibrator was revisited, which allowed for accurate gain amplitude, phase and polarization leakage calibration. This reuslts in the RR, RL, LR and LL visbilities that encodes the antenna primary beam for those correlations. Further using the scanning and tracking antenna gains and leakage tables we derived the antennas Jones matrix patterns that were used in this analysis.

2.1.2 ALMA

Calibration was carried out using the ALMA Polarization calibration guide[1] as a template based on which a holography calibration script was generated. The script closely follows the calibration steps carried out by the ALMA polarization beam characterization report[2], with the difference being we use the calibration tasks and tools within CASA[3]. In short, the calibration process is removing affects on the signal chain, leaving the calibrated data to only contain the affects of instrumental polarization so it can be properly measured. These are the steps:

- A-priori flagging
- Water vapor measurement corrections

[1] https://casaguides.nrao.edu/index.php/3C286_Band6Pol_Calibration_for_CASA_4.3
[2] http://www.alma.cl/ skameno/AMAPOLA/PolarizedBeamProc.html
[3] version used for processing the data is the 5.3 release

- Combine executions for greater parallactic angle coverage
- Determine short-duration atmospheric gains (pre-bandpass)
- Determine antenna-based frequency gains (bandpass)
- Determine back-end electronics gains (cross-hand gains)
- Determine each antenna's XY-phase offset
- Recompute antenna gains now that source polarization is accounted for
- Determine polarization contribution of each antenna
- Apply the calibration tables.
- Flag any poorly behaving antennas (iterative process)

2.1.3 MeerKAT

We used the MeerKAT holography data obtained by Mattieu de Villiers and the MeerKAT commissioning team at SARAO, Cape Town. In this case, a spiral pattern was followed while observing a bright calibrator source. The holography was observed with reduced spectral resolution (1024 channels across the band rather than the native 4096) using 18 antennas in the array. The pointings observed on the spiral are interpolated on to a regular grid, however the noise characteristics are not uniform across this grid. This does not materially affect our results from the Zernike modeling.

Chapter 3

Zernike Modeling process

The Zernike polynomials, which are defined to be orthogonal on a unit circle, are fit to the measured holography in the aperture plane, as any optical aberrations are most naturally modeled in this domain. Any blockages to the aperture, off-axis feeds, an offset illumination *etc.* will cause distortions and rotation asymmetries in Stokes-I, and can cause a squint between the Stokes Q and U beams. Rather than model the primary beam itself, we model the aperture plane as a series of Zernike polynomials and show that capturing these details allows us to reconstruct the full Stokes antenna primary beam to high accuracy.

The aperture illumination is obtained from a Fourier transform (FT) of the antenna far-field voltage pattern. The measured holography data is resampled/interpolated on to a regular grid - a direct FT of this grid will lead to aliasing in the aperture domain due to the implicit rectangular window imposed on the sampled data. In order to avoid aliasing, the data are padded by a factor of 10 prior to the FT. This then leads to the padded aperture plane, which is trimmed to an appropriate size that reflects the physical dimensions of the antenna dish. The advantage of modeling the aperture domain is that the maximum dimensions are determined by the telescope in question and not by the number of sidelobes measured in the holography.

The aperture obtained in this manner is a convolution of the FT of the rectangular window, *i.e.,* the 'sampling PSF', and the "true" aperture, and therefore needs to be deconvolved prior to fitting. We employ a simple Fourier-based linear deconvolution method to remove the effects of the sampling PSF. We model the aperture plane using the first ten orders of Zernike polynomials *i.e.,* a total of 66 polynomials. This is a fairly arbitrary limit, and might be revised in the future. The initial input to the fitter assigns a weight of unity to all the Zernike terms. The fitter is a non-linear least squares solver that uses the Levenberg-Marquardt algorithm, which modifies the weights associated with each term to obtain the best fit surface. The model PB is generated in a manner similar to what is described above, *i.e.,* padding and FT-ing the model aperture. Care must be taken to keep track of normalization across Fourier transforms in order to preserve the absolute scale.

This procedure is repeated for every channel and Jones/Stokes measurement in the data, yielding a frequency dependent aperture model that captures the wideband behaviour of the PB. For example, we caputure the well known 17 MHz resonance observed in the peak of the VLA PB. In principle, this allows us to proceed with a full Stokes, wide band AW projection.

The efficacy of the fitting is independent of the telescope, dish type, and feed basis. The success of the method hinges on having well-sampled holography data. Figures 3.1 – Figure 3.5 show the measured data, the Zernike model and the residual in the PB domain. The expected patterns are reproduced accurately, *i.e.* the clover leaf pattern for the cross hand Jones and the off-axis asymmetries for the parallel hand Jones/Stokes I beams. Note that the plots shown in Figures 3.3 – 3.5 show the Stokes I beam, and the leakage from I into Q, U, and V respectively. The Stokes I beam has been normalized such that the peak is 1.

This modeling procedure allows us to capture the antenna PB as a weighted sum of analytic functions. Given that the W term is also analytic, we can then generate the AW term at a much reduced computational cost as compared to the earlier ray tracing method. This problem is embarassingly parallel, and should scale well across GPUs/clusters.

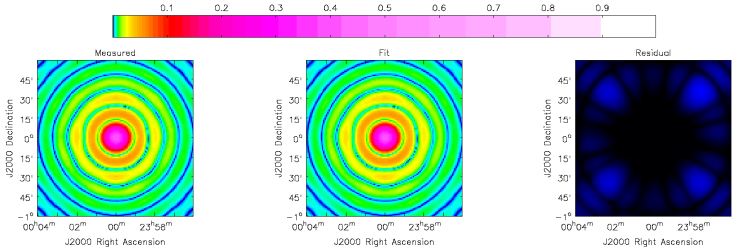

(a) X Jones

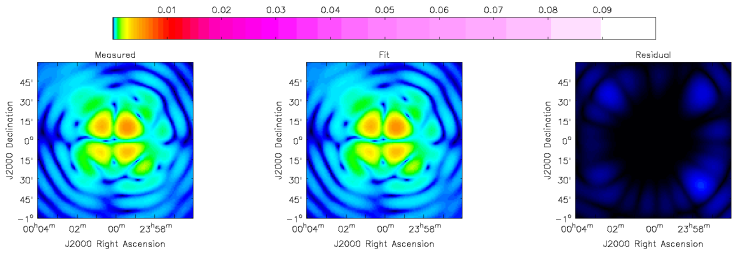

(b) X → Y Jones

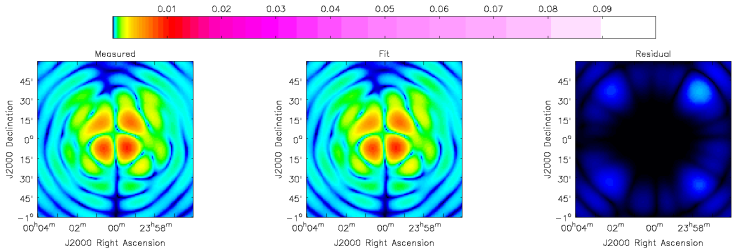

(c) Y → X Jones

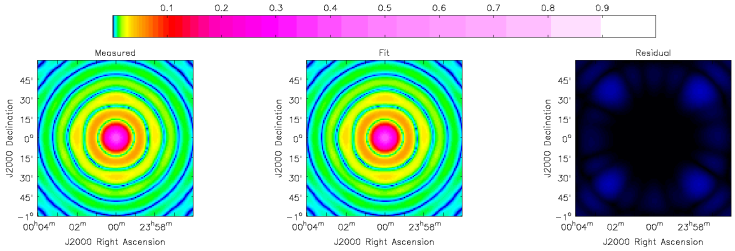

(d) Y Jones

Figure 3.1: Zernike modeling of the MeerKAT PB. From left to right, the measured PB, the model PB and the residuals. The Zernike models capture the PB structure in all polarizations very well out to the third sidelobe. Note that the scale is different for the parallel-hand and cross-hand plots. Plotted here is a single channel (at 1284 MHz) from the wideband holography.

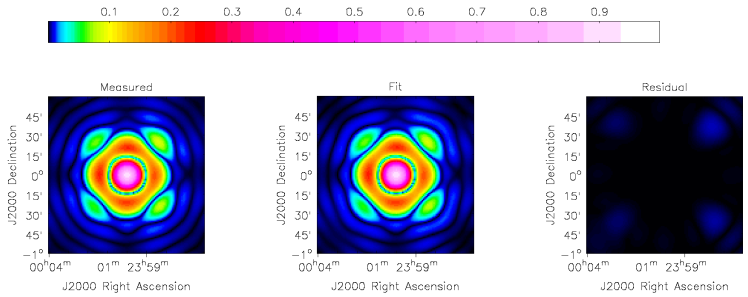

(a) R Jones

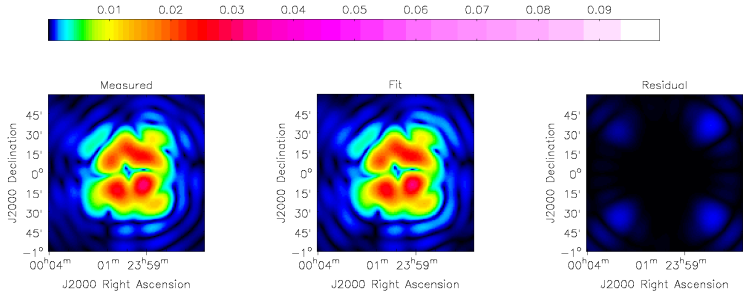

(b) R → L Jones

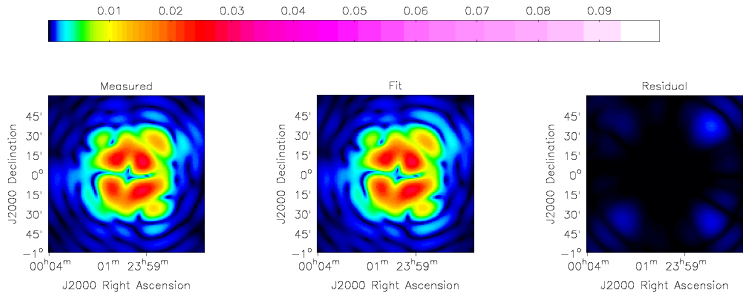

(c) L → R Jones

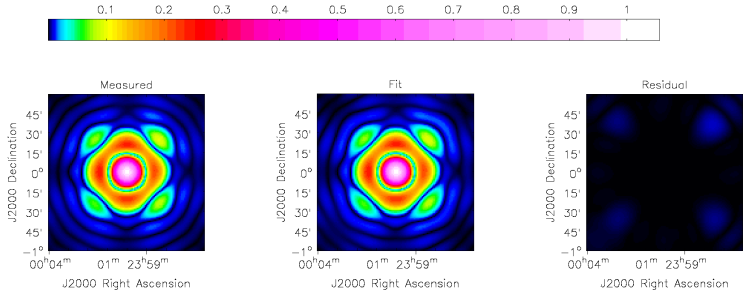

(d) L Jones

Figure 3.2: Zernike modeling of the VLA L band PB. From left to right, the measured PB, the model PB and the residuals. The Zernike models capture the PB structure in all polarizations very well out to the third sidelobe. Note that the scale is different for the parallel-hand and cross-hand plots. Plotted here is a single channel (at 1050 MHz) from the wideband holography.

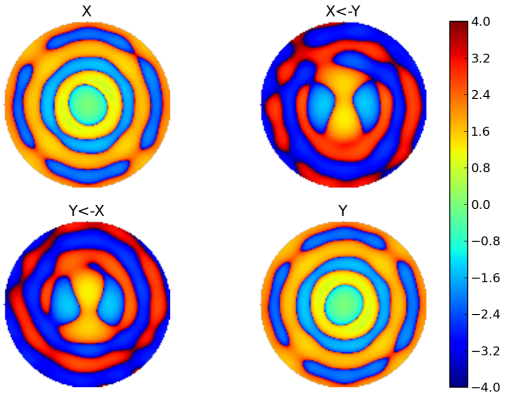

(a) Jones data, ALMA DA dish

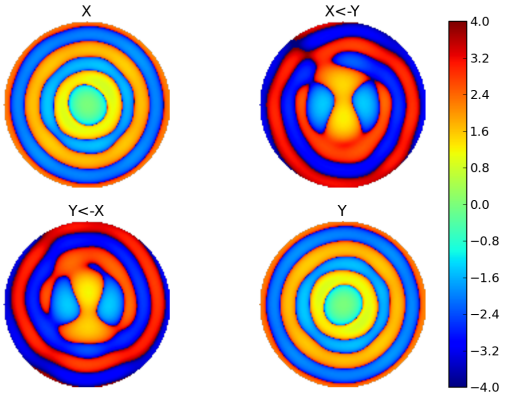

(b) Jones model, ALMA DA dish

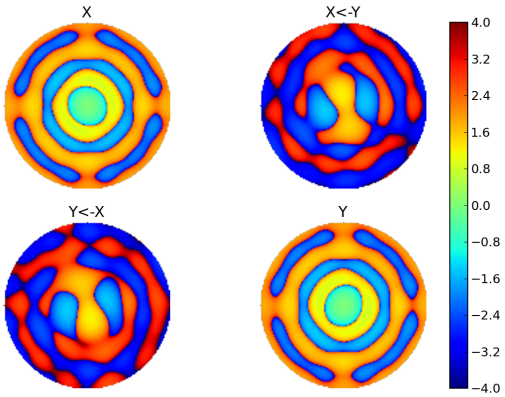

(c) Jones data, ALMA DV dish

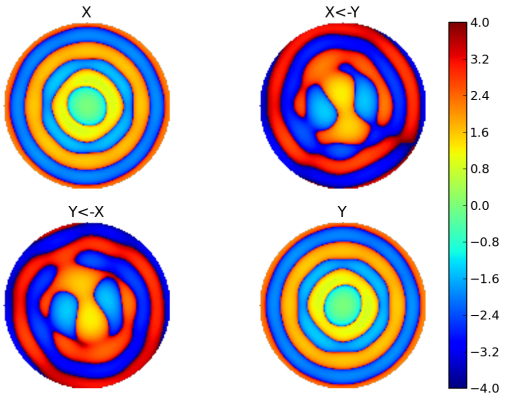

(d) Jones model, ALMA DV dish

Figure 3.3: Zernike modeling of the ALMA Stokes measurements. Plotted here is the data from a single channel at 100 GHz. The data (left column) and model (right column) are plotted on a log scale. The scale limits are from -10^{-4} to 10^{-4} (-4 and 4 on the colorbar). Regions shaded saturated blue and red share the same value (*i.e.,* 10^{-4}) but have a flipped sign. The subplots show the Stokes I beam, and the leakage of Stokes I into Stokes Q, U, and V.

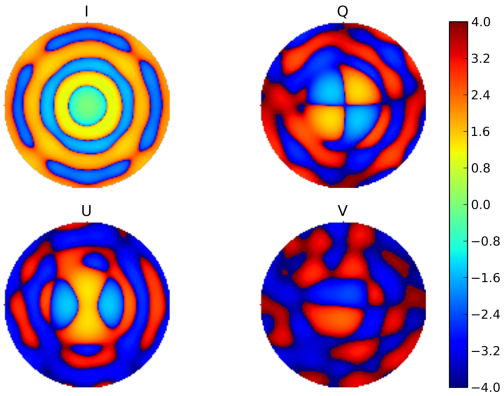

(a) Stokes data, ALMA DA dish

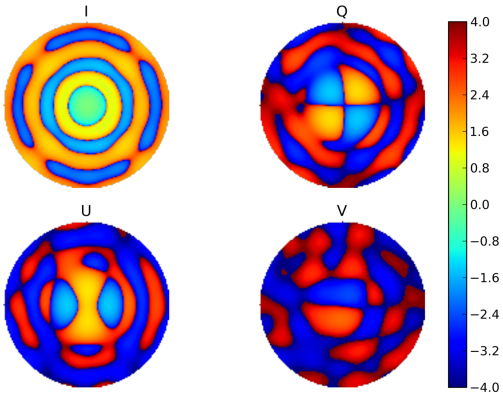

(b) Stokes model, ALMA DA dish

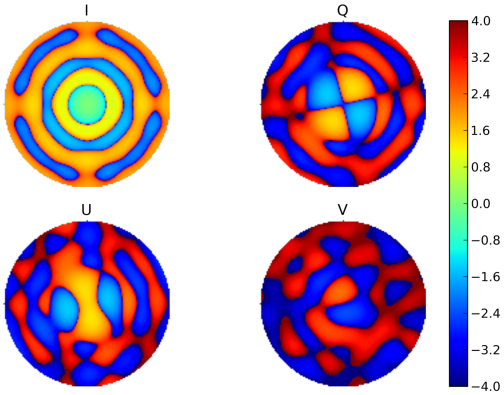

(c) Stokes data, ALMA DV dish

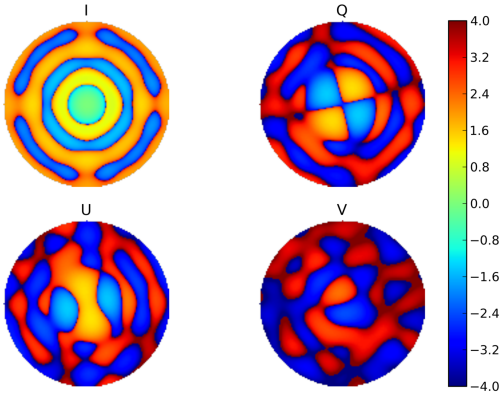

(d) Stokes model, ALMA DV dish

Figure 3.4: Zernike modeling of the ALMA Stokes measurements. Plotted here is a single channel at 100 GHz. The data (left column) and model (right column) are plotted on a log scale. The scale limits are from -10^{-4} to 10^{-4} (-4 and 4 on the colorbar). Regions shaded saturated blue and red share the same value (*i.e.,* 10^{-4}) but have a flipped sign. The subplots show the Stokes I beam, and the leakage of Stokes I into Stokes Q, U, and V.

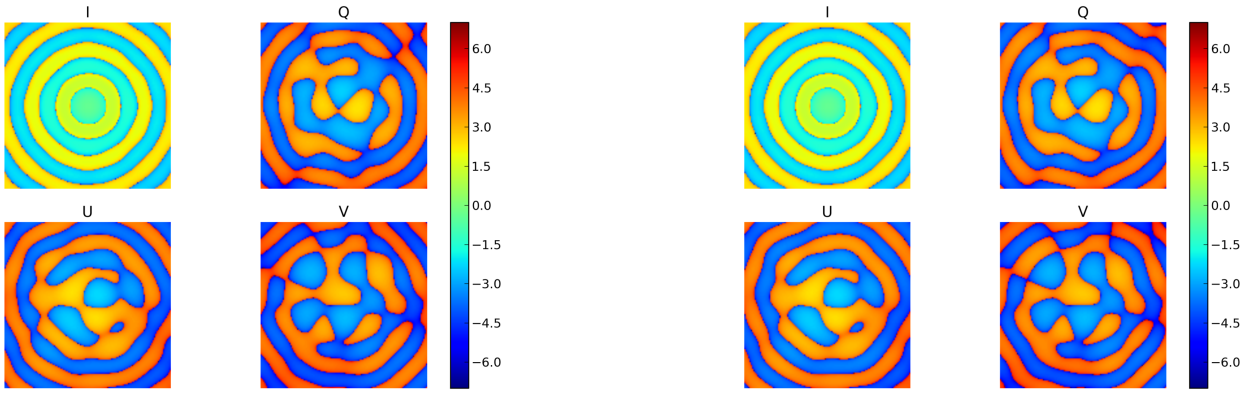

(a) Stokes data, MeerKAT

(b) Stokes model, MeerKAT

Figure 3.5: Zernike modeling of the MeerKAT Stokes measurements. Plotted here is a single channel at 1284 MHz. The data (left column) and model (right column) are plotted on a log scale. The scale limits are from -10^{-6} to 10^{-6} (-6 and 6 on the colorbar). Regions shaded saturated blue and red share the same value (*i.e.,* 10^{-6}) but have a flipped sign. The subplots show the Stokes I beam, and the leakage of Stokes I into Stokes Q, U, and V.

Bibliography

Bhatnagar, S., Cornwell, T., Golap, K., & Uson, J. M. 2008, Astronomy & Astrophysics, 487, 419

Jagannathan, P. 2018, PhD thesis, University of Cape Town

Jagannathan, P., Bhatnagar, S., Brisken, W., & Taylor, A. 2017, The Astronomical Journal, 155, 3